Engineering Colossal Anisotropic Thermal

Expansion into Organic Materials through

Dimensionality Control

Navkiran Juneja, Daniel K. Unruh, and Kristin M. Hutchins*

Department of Chemistry and Biochemistry, Texas Tech University, 1204 Boston Avenue,

Lubbock, Texas 79409, United States. Email: kristin.hutchins@ttu.edu

ABSTRACT

Thermal expansion (TE) behavior in solid-state materials is influenced by both molecular and

supramolecular structure. For solid-state materials assembled through covalent bonds, such as

carbon allotropes, solids with higher dimensionality (i.e., diamond) exhibit less TE than solids

with lower dimensionality (e.g., fullerene, graphite). Thus, as the dimensionality of the solid

increases, the TE decreases. However, an analogous and systematic variation of the dimensionality

in solid-state materials assembled through noncovalent bonds with correlation to TE has not been

studied. Here, we designed a series of solids based on dimensional hierarchy to afford materials

with zero-dimensional (0D), 1D, and 2D hydrogen-bonded structures. The 2D materials are

structural analogs of graphite and covalent-organic frameworks, and we demonstrate that these 2D

1

solids exhibit unique biaxial zero TE with anisotropic and colossal TE along the π -stacked direction ($\alpha \sim 200 \, \text{MK}^{-1}$). The overall behavior in the 2D hydrogen-bonded solids is similar to 2D covalent-bonded solids; however the coefficient of TE along the π -stacked direction for these hydrogen-bonded solids is an order of magnitude higher than in 2D graphite or phosphorous allotropes. The hierarchal materials design strategy and correlation to TE properties described herein can be broadly applied to design and synthesis of new solid-state materials sustained by covalent or noncovalent bonds with control over solid-state behaviors.

INTRODUCTION

Modulating the solid-state property of thermal expansion (TE), which describes the response of a material to a change in temperature, ¹⁻⁴ is of utmost importance for fabricating materials with extraordinary performance. ⁵⁻⁹ Depending on the intended application, specific TE behaviors are often required. For example, materials that exhibit large TE behavior are useful for thermomechanical actuators and sensors. ¹⁰⁻¹² On the other hand, materials that undergo smaller changes in response to temperature alterations are useful in ceramics and aerospace applications. ¹³, ¹⁴ In the field of semiconductor and composite materials, the TE behavior of all the components needs to be adequately matched to avoid device failure when temperature changes occur. ¹⁵⁻¹⁷ One significant challenge that materials scientists face lies in controlling a material's structure, and this control is critical because structure directly influences properties. ¹⁸⁻²³ Control over solid-state structure is often accomplished by directing atomic or molecular self-assembly and packing in all dimensions. ²⁴⁻²⁹ However, depending on the atomic or molecular building blocks, some dimensions may not be easily self-assembled with assistance from strong interactions.

The property of TE in solid materials is often dictated by the strength of the bonds that lie along each direction. Stronger bonds are typically less affected by temperature when compared to weaker ones.³⁰ Specifically, in carbon allotropes, which are sustained by covalent bonds, TE decreases as the dimensionality increases, i.e., fullerene (0D) > graphite (2D) > diamond (3D). 31-35 While diamond exhibits minimal overall TE, graphite exhibits anisotropic, uniaxial TE along the stacking direction. Carbon also exists in the form of carbon nanotubes (1D); however, TE behavior of the 1D form depends on the length and thickness variations in the nanotubes. Analogous to carbon, phosphorus also exists as several allotropes including white (0D), red (1D), blue (2D), and black (2D).³⁶ The two 2D allotropes comprise infinite stacks of phosphorene layers that interact via van der Waals forces, and TE behavior for the 2D allotropes has been explored computationally. 37-39 Calculations show that the armchair direction of phosphorene in black phosphorus is more expandable as compared to the zig-zag direction of phosphorene in the blue phosphorus allotrope.³⁷ The TE behavior for 2D black phosphorous has also been investigated experimentally and anisotropic, uniaxial expansion occurs between phosphorene layers, similar to graphite. 40, 41 The 2D allotropes of carbon and phosphorous, as well as other 2D solids such as silicene, transition-metal dichalcogenides, hexagonal boron nitride, and covalent-organic frameworks (COFs), have attracted significant attention for their electronic, optical, and thermal properties.²⁴, 42-45

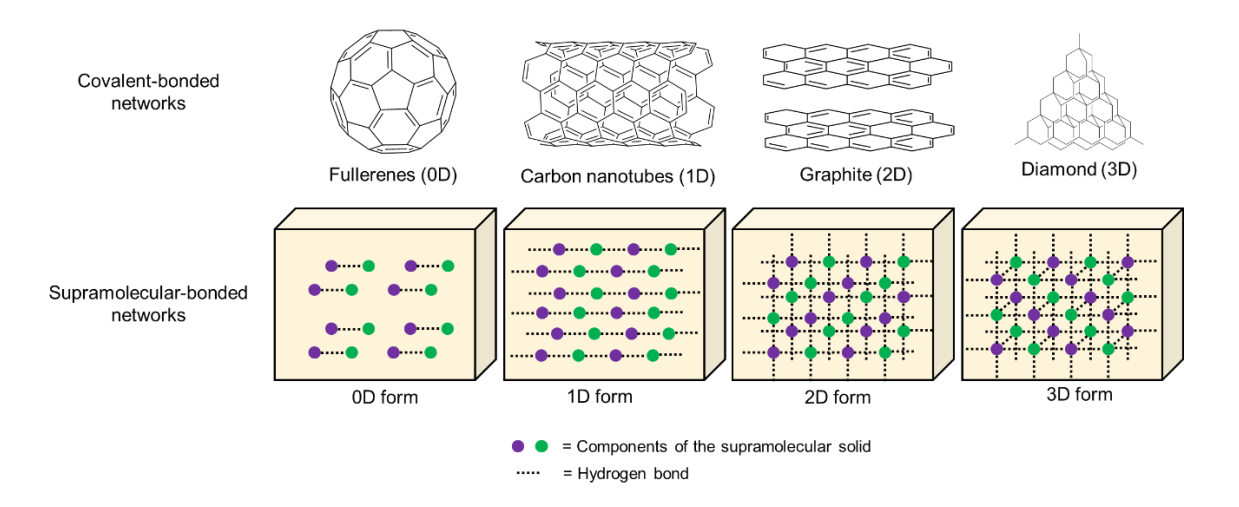


Figure 1. Supramolecular-bonded networks prepared through self-assembly of components, which are analogous to covalent-bonded networks such as carbon allotropes. In this study, the dashed lines represent hydrogen bonds between components.

Solid materials that exhibit different dimensionalities is not unique to covalently-bonded solids (e.g., carbon allotropes). Organic compounds can also be assembled into solid networks of differing dimensionality, but held together through noncovalent bonds (Figure 1). TE behavior in such organic solids is dictated by the strength of the weaker, noncovalent interactions lying along each direction and can be anisotropic.^{4, 46, 47} For example, the simple carboxylic acids, 2-butynoic acid and oxalic acid are each known to crystallize in two different forms that differ in the dimensionality of intermolecular hydrogen bonding (0D to 2D). 2-Butynoic acid crystallizes in a 0D and 1D form, and the 1D form exhibits lower TE.⁴⁸ Oxalic acid crystallizes in 1D and 2D forms, and the 2D form exhibits slightly lower TE.⁴⁹ For multi-component organic solids, similar TE behavior has been observed in polymorphs that both contain hydrogen bonds in 1D.⁵⁰ As outlined above, correlation of structural dimensionality to TE behavior has been explored for carbon allotropes;^{32, 35, 51, 52} however, an analogous investigation for molecular solids assembled through noncovalent bonds has not been conducted.

We set out to design and synthesize a series of solid materials wherein the dimensionality was systematically increased from 0D to 1D to 2D (Figure 1). We hypothesized that as the supramolecular-bonding dimensionality is increased from 0D to 2D, the TE will decrease. We chose to use hydrogen bonds to facilitate self-assembly because hydrogen bonds are directional, robust, and one of the most widely used supramolecular interactions, thus, broadening the applicability of our strategy. We expected that the directions along which the strong hydrogen bonds lie in each solid would exhibit the least TE and larger expansion would occur along the other directions (without strong hydrogen bonds). Thus, the 2D solids, which are structurally analogous to graphite and COFs, may exhibit minimal expansion in two dimensions and significant expansion, anisotropically, along the third dimension.

Here, we demonstrate for the first time that controlling self-assembly and structure dimensionality in supramolecular solids affords control over TE behavior in a manner analogous to covalently-bonded solids/allotropes. By increasing the hydrogen-bonding dimensionality from 0D to 1D to 2D, the TE decreases along the direction of the strong hydrogen bonds. The 2D solids described here are directly relevant to graphite, COFs, and other 2D materials. In these 2D hydrogen-bonded materials, we, perhaps surprisingly, achieve near zero TE within the hydrogen-bonded sheets and colossal, anisotropic TE along the π -stacked direction. This biaxial zero TE and anisotropic TE behavior is similar to graphite and black phosphorous; however the uniaxial TE coefficients for the 2D hydrogen-bonded solids here are an order of magnitude larger than graphite and 2D phosphorous and on par with or higher than some of the highest reported TE coefficients for multi-component supramolecular solids. The hierarchical approach to solid-state supramolecular materials design described here is broadly applicable toward design of novel

materials with tunable properties. Morevoer, our design strategy demonstrates how anisotropic behaviors can be engineered into solid-state materials.

EXPERIMENTAL SECTION

We selected aromatic carboxylic acids as the hydrogen-bond-donor molecules and bipyridines as hydrogen-bond acceptors. Three carboxylic acids that would afford solids of different dimensionalities were chosen, namely, benzoic acid (BA), terephthalic acid (TA), and trimesic acid (TMA). Three hydrogen-bond-accepting bipyridines including 4,4′-azopyridine (azo), 1,2-di(4-pyridyl)ethylene (bpe), and 1,2-bis(4-pyridyl)ethane (bpeth) were also selected. Cocrystallization of bipyridines with: BA would yield 0D hydrogen-bonded units, TA would afford infinite 1D hydrogen-bonded chains, and TMA would result in 2D hydrogen-bonded sheets (Figure 2). The dimensionality of each solid (0D, 1D or 2D) is defined by the COO-H···N hydrogen bonds that direct the self-assembly of the carboxylic acid and pyridine molecules. Our group has already investigated the TE behavior of the 1D solids. Here, we use the previously reported TE data for the 1D solids and compare it to the new 0D and 2D solids synthesized here. It is of interest to note that the N=N and C=C groups within azo and bpe, respectively, are capable of undergoing conformational interconversion (often termed molecular pedal motion) in the crystalline state, 53 which has been shown to affect TE, 54, 55

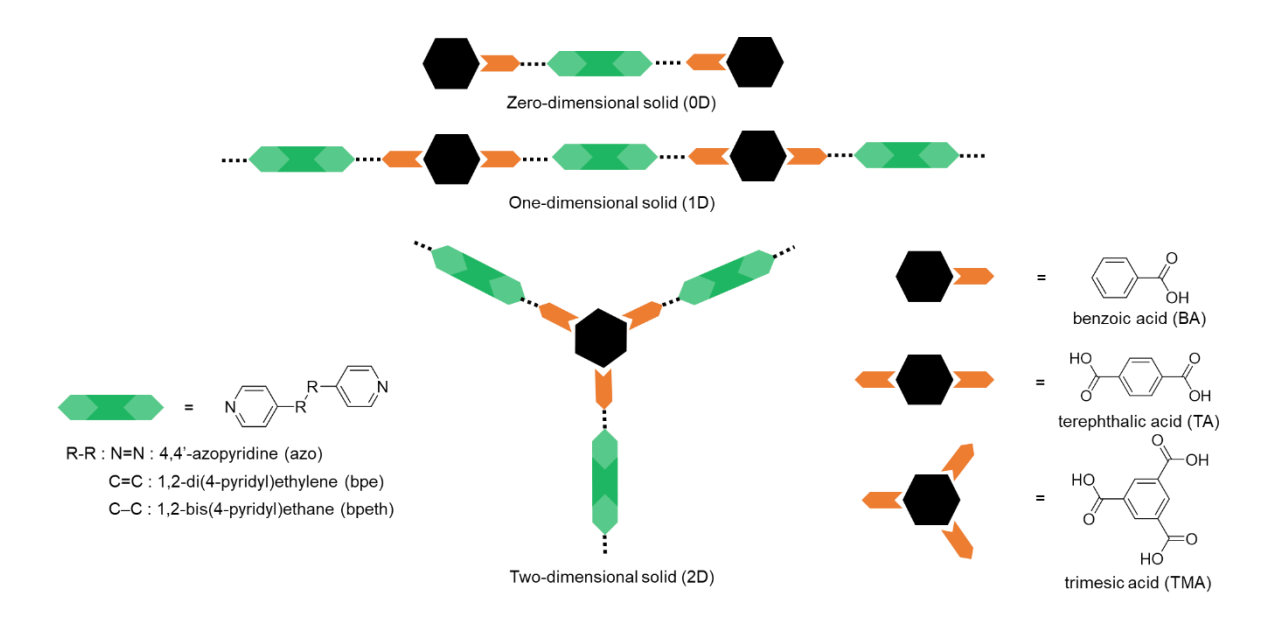


Figure 2. Hydrogen-bond-acceptor and -donor molecules used to prepare solids with increasing hydrogen-bonding dimensionality (0D to 2D).

To investigate the structural response of each solid to temperature change, variable-temperature X-ray diffraction data is needed. Thus, crystals of each solid suitable for single-crystal X-ray diffraction were prepared using slow evaporation techniques. An appropriate molar ratio of the two components for each solid was dissolved in an organic solvent and the solution was left to evaporate slowly (see ESI for individual experimental details). Some of the 0D and 2D solids have been previously described (noted in each section if so), but no variable temperature data has ever been reported. Variable-temperature single-crystal X-ray diffraction (VT-SCXRD) experiments were performed for each multi-component solid over the temperature range of 190-290 K, and a full data set was collected every 20 K (Table S1-S14). The bulk material was characterized by ¹H NMR spectroscopy (Figure S8-S14) and powder X-ray diffraction (Figure S15-S23). The molar ratios of the components within each solid were confirmed by SCXRD data and ¹H NMR spectroscopy. PASCal⁵⁶ was used to calculate the principal axes of TE (X₁, X₂, and X₃) and the TE coefficients for each solid using the VT-SCXRD data (Figure S1-S7, Table S15). The program

Mercury was used to correlate the principal axes of TE to the solid-state structure. The changes in unit cell lengths as a function of temperature were also calculated for each solid (Figure S24-S30).

RESULTS AND DISCUSSION

OD solids

The multi-component solids prepared using BA as the hydrogen-bond donor all self-assemble into 0D hydrogen-bonded units, as designed. Two structural forms (i.e., polymorphs) were obtained for the 0D solids containing BA and azo (BA·azo Form-I and BA·azo Form-II). The two polymorphs contain the components in the same ratio; thus, the NMR spectra appear nearly the same. However, powder X-ray diffraction characterization successfully confirmed the polymorphism in the bulk materials, and preparation of each polymorph was controlled by the solvent used for crystallization (Figure S15). The 0D solids containing BA and bpe (BA·bpe) or bpeth (BA·bpeth) have been reported previously.⁵⁷ Here, we obtained identical solids and conducted VT-SCXRD experiments for the first time.

The asymmetric unit for all the BA-based solids contains one molecule of BA and one half of a molecule of the bipyridine. The components self-assemble into a discrete 0D unit via COO-H···N and C-H(α)···O hydrogen-bonded dimers as expected (Table S16-S18 for bond distances). In BA·azo Form-I, BA·bpe, and BA·bpeth, the adjacent 0D units interact via C-H···O interactions to form a sheet (Figure 3a, 4a, 4c). On the other hand, in BA·azo Form-II, the adjacent chains are twisted by 53° and interact via C-H···O and C-H···N interactions to form a sheet in an ABAB sequence (Figure 3c). In all the 0D solids, the sheets stack via offset face-to-face π ··· π interactions (Figure 3b, 3d, 4b, 4d). In BA·bpe, the C=C bridge of the bipyridine is disordered over two

positions at every temperature. The disorder is static as the site occupancies of the C=C bond remain nearly constant over the temperature range of 190-290 K (Table S20).

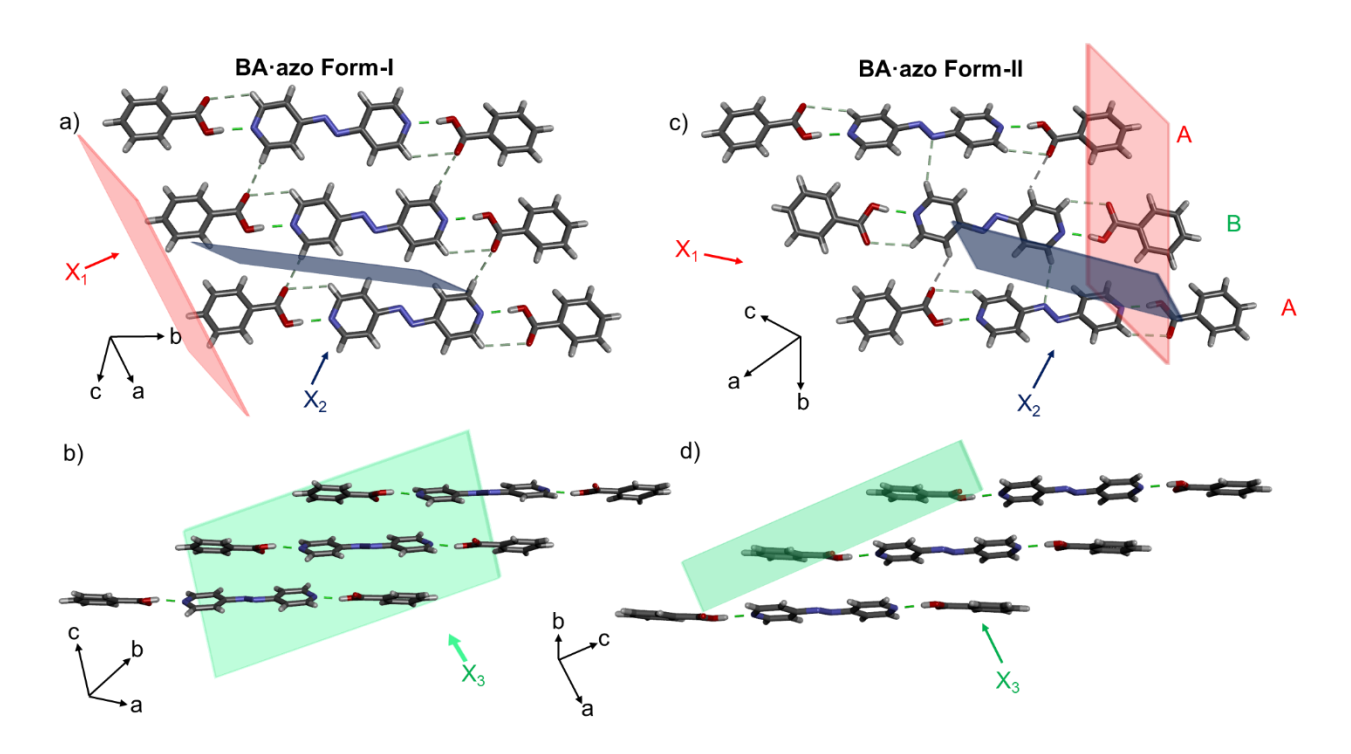


Figure 3. Single crystal X-ray structures at 290 K highlighting adjacent 0D units and π stacks within (a,b) BA·azo Form-I and (c,d) BA·azo Form-II. The hydrogen bonds are shown with dashed lines; COO-H···N are green while C-H···O and C-H···N are grey. The TE axes X_1 (red), X_2 (blue), and X_3 (green) are highlighted by planes and arrows.

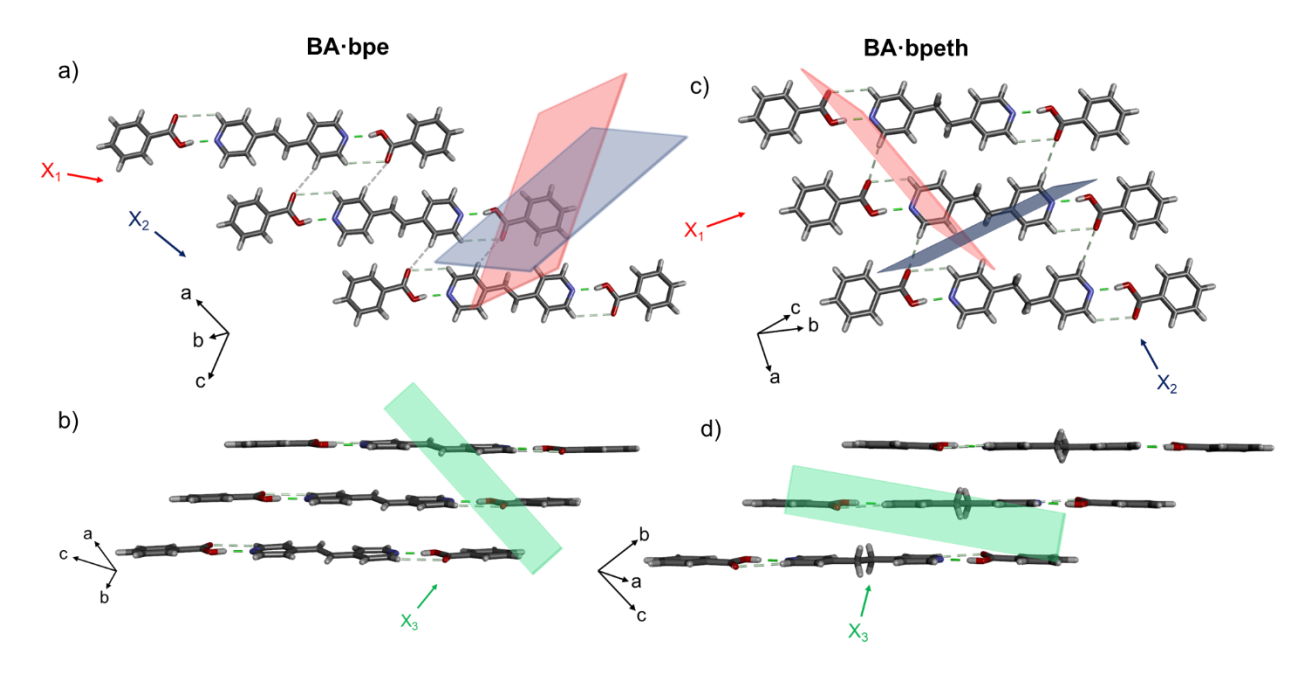


Figure 4. Single crystal X-ray structures at 290 K showing adjacent 0D units and π stacks within (a,b) BA·bpe and (c,d) BA·bpeth. The hydrogen bonds are shown with dashed lines; COO-H···N are green while C-H···O are grey. The TE axes X_1 (red), X_2 (blue), and X_3 (green) are highlighted by planes and arrows. Disorder has been omitted for clarity.

1D solids

Solids of TA with azo, bpe, and bpeth have been previously reported by our group. The two components in each solid self-assemble into infinite 1D chains via COO-H···N and C-H(α)···O hydrogen-bonded dimers. The adjacent chains interact via C-H···O hydrogen bonds to form a sheet, and the sheets pack into face-to-face π -stacked layers. None of the 1D solids showed evidence of molecular pedal motion⁵⁸ (Figure 5).

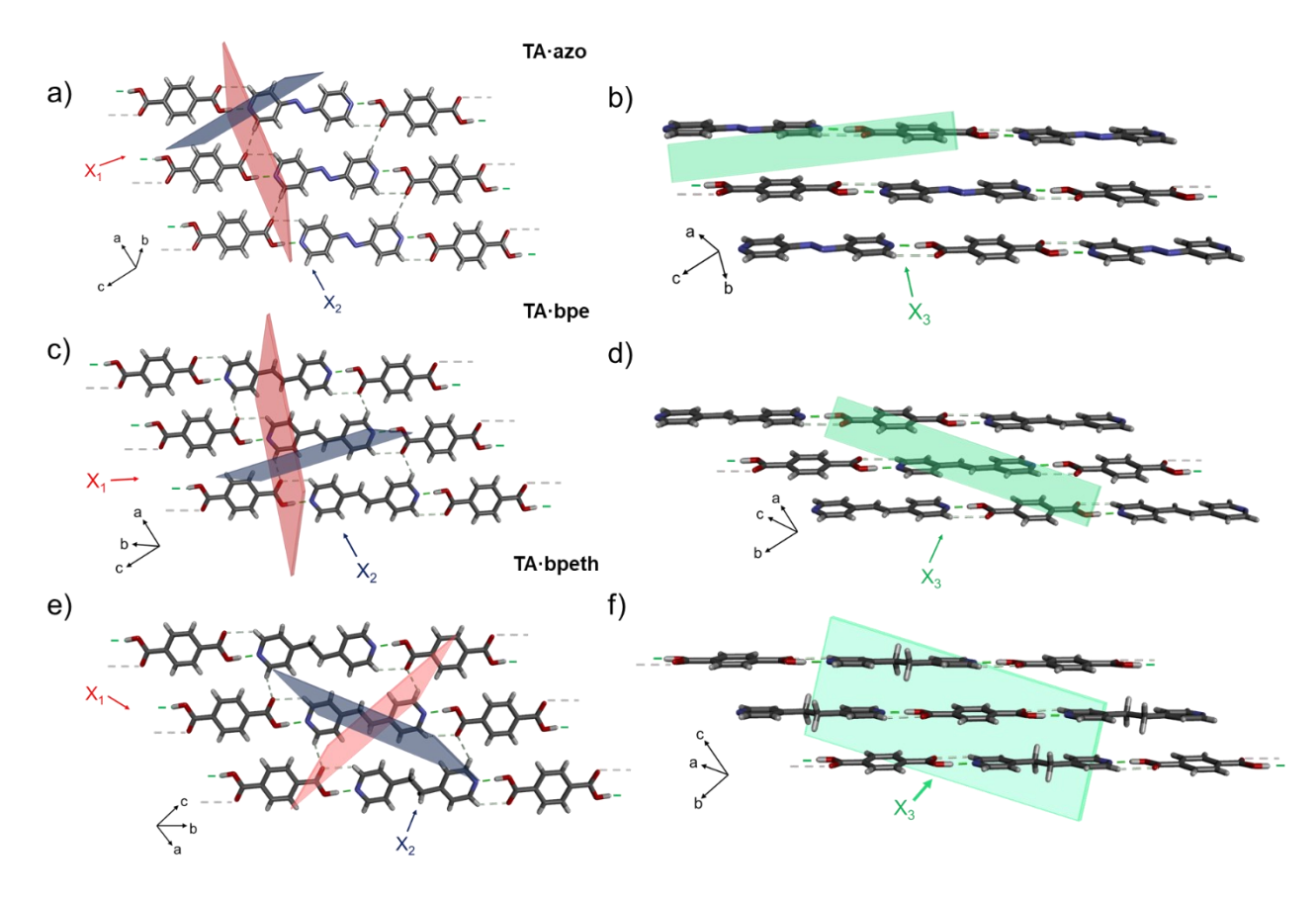


Figure 5. Single crystal X-ray structures at 290 K highlighting adjacent 1D chains and π stacks within (a,b) TA·azo, (c,d) TA·bpe, and (e,f) TA·bpeth. The hydrogen bonds are shown with dashed lines; COO-H···N are green while C-H···O are grey. The TE axes X_1 (red), X_2 (blue), and X_3 (green) are highlighted by planes and arrows.

2D solids

The multi-component solids prepared using TMA as the hydrogen-bond donor all self-assemble into 2D hydrogen-bonded sheets as designed. The components of TMA·azo crystallized in 1:2 ratio, and both crystallographically unique azo molecules exhibit disorder during the variable temperature experiment. The site occupancies in the azo molecules change by 21% and 17% over the temperature range of 190-290 K indicating dynamic conformational interconversion (motion) in the solid (Table 1). The solid TMA·bpe and two polymorphs of TMA·bpeth have been

previously reported.^{57, 59} Here, we obtained isostructural solids of TMA·bpe and TMA·bpeth (form 1) and conducted VT-SCXRD experiments for the first time. The components of TMA·bpe and TMA·bpeth crystallized in a 2:3 ratio. Both crystallographically unique bpe molecules in TMA·bpe also exhibit disorder during the variable temperature study. However, the overall changes are significantly smaller (6% and 4%) when compared to the solid with azo (Table 1). One of the bpeth molecules in TMA·bpeth is also statically disordered (Table S21).

Table 1. Major site occupancies for two crystallographically unique azo and bpe molecules in the 2D solids over the temperature range 190-290 K. The minor site is equal to 100-the major site. The error is shown in parenthesis.

Temperature (K)	Major site occupancy (%)			
	azo (1)	azo (2)	bpe (1)	bpe (2)
190	91 (1)	100	64 (1)	100
210	88 (1)	100	63 (1)	100
230	84 (1)	97 (1)	62 (1)	100
250	80 (1)	95 (1)	61 (1)	100
270	75 (1)	90 (1)	59 (1)	97 (1)
290	70 (1)	83 (1)	58 (1)	96 (1)

The components in all three solids self-assemble into a 2D honeycomb grid sustained by COO-H···N and C-H(α)···O hydrogen-bonded dimers (Figure 6). Some C-H···N interactions between adjacent azo molecules also aid in the formation of the hexagonal grid in TMA·azo. The internal dimensions of the hexagonal cavities are 42 x 29 Å for TMA·azo, 46 x 31 Å for TMA·bpe, and 46 x 32 Å for TMA·bpeth. However, this cavity space is filled by the extended packing of the

hexagonal layers; thus, there is no void space in the solids (Figure S32). The 2D sheets self-assemble into π -stacked layers.

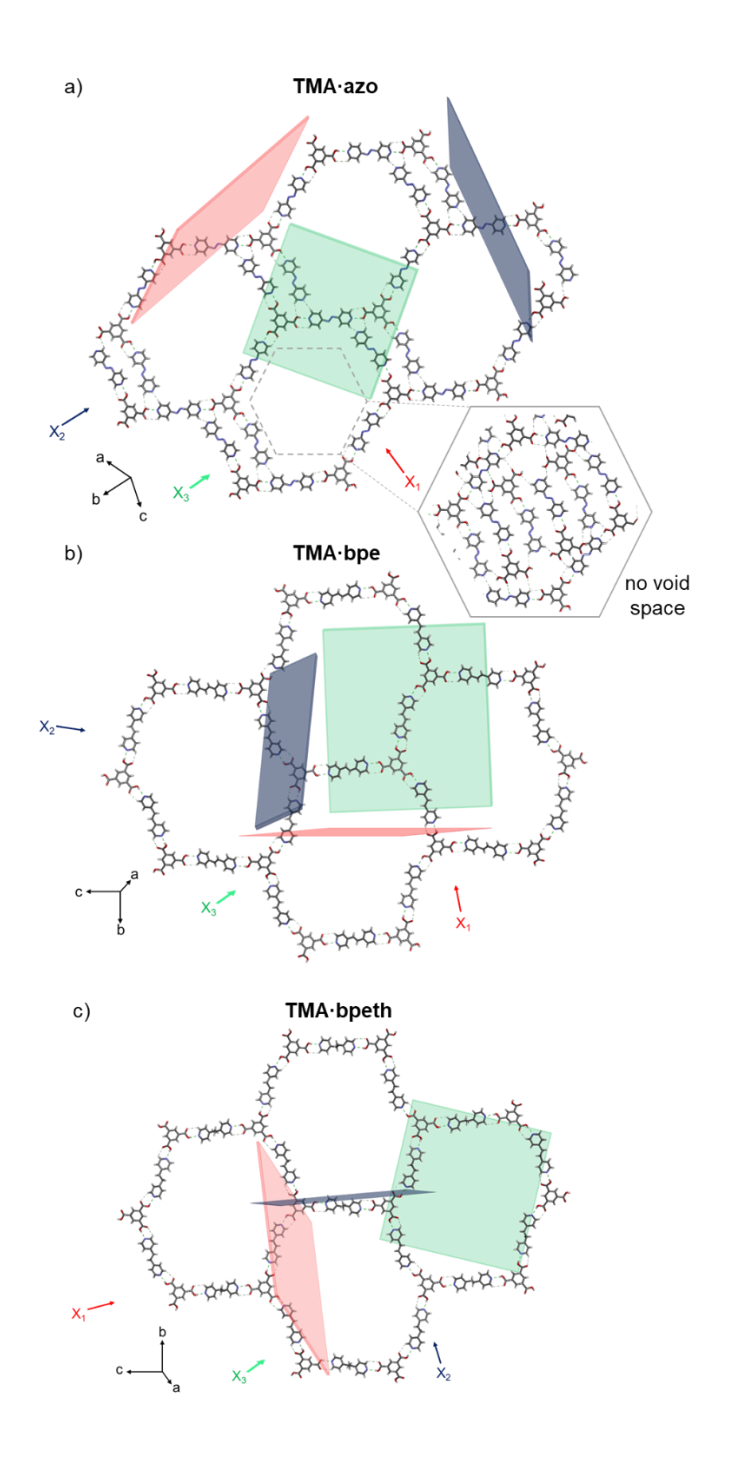


Figure 6. Single crystal X-ray structures at 290 K showing hexagonal 2D sheet in a) TMA·azo, b) TMA·bpe, and c) TMA·bpeth. The hydrogen bonds are shown with dashed lines; COO-H···N are green while C-H···O and C-H···N are grey. The TE axes X_1 (red), X_2 (blue), and X_3 (green) are highlighted by planes and arrows. The cavities in all three solids are densely packed and hence there is no void space. The cavity of TMA·azo is shown in part a as an example. Disorder has been omitted for clarity.

Thermal expansion behaviors

To investigate the impact of dimensionality on TE behavior, the TE coefficients (α_{X1} , α_{X2} , and α_{X3}) and the directions of the principal axes of TE (X_1 , X_2 , and X_3) were calculated using the software, PASCal (Figure 7, Table S15). TE along X_1 is the least (or most negative), while TE along X_3 is the largest positive value. Most materials expand upon heating (positive TE, PTE), and very rarely, materials contract overall (negative TE, NTE) or undergo nearly no overall change (zero TE, ZTE) upon heating. TE is currently defined as 'colossal' if the coefficient is ≥ 100 MK¹. Figures 3-6 above highlight the directions of the principal axes of TE with respect to the solid-state structure.

Although hydrogen bonds are weaker than covalent bonds, our group and others have shown that TE along hydrogen bonds can be minimized in solid materials. Given our design of 0D, 1D, and 2D hydrogen-bonded solids, we expected limited TE in the directions where the strong (COO-H····N) hydrogen bonds lie. Thus, the 1D solids are expected to exhibit minimal TE in one dimension, while the 2D solids were expected to be limited in two dimensions.

In all of the 0D solids, mild PTE or near ZTE occurs along X_1 , which does indeed lie along the direction of the hydrogen-bonds within the 0D units (Figures 3 and 4). In the 1D solids, ZTE or

NTE occurs along X_1 , which is also the direction of the 1D hydrogen-bonded chains (Figure 5). Thus, the TE is limited along X_1 in both the 0D and 1D solids. TE along X_2 is larger for all the 0D and 1D solids, ranging from mild to moderate PTE.

In all of the 2D solids, ZTE or NTE occurs along both X_1 and X_2 , which lie along the directions of the hydrogen-bonded sheet (Figure 6). In the 2D solids, the NTE or ZTE also coincides approximately with the b and c axes (Figure S26, S28, and S30). In all the solids, regardless of the dimensionality, colossal PTE occurs along X_3 because this third dimension is sustained by weaker noncovalent bonds, specifically, π stacking (Figure 7).

Overall, the major differences in the TE between the solids is observed along X_2 and X_3 . The 0D and 1D solids exhibit moderate PTE and colossal PTE along X_2 and X_3 , respectively, because strong hydrogen bonds only lie along X_1 . The 2D solids exhibit ZTE and anisotropic colossal PTE along X_2 and X_3 , respectively, because strong hydrogen bonds lie along X_1 and X_2 . Thus, in the 2D solids, because of the biaxial zero TE, the anisotropic colossal expansion along X_3 is directly responsible for the volumetric expansion as well.

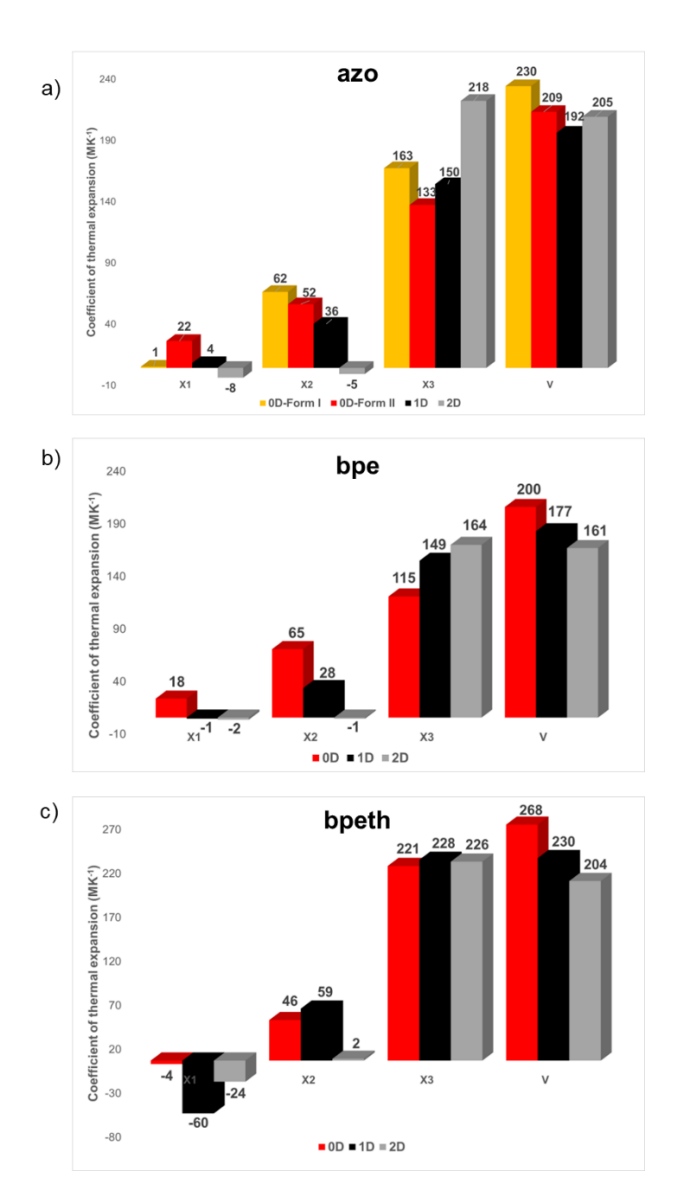


Figure 7. Linear (X_1, X_2, X_3) and volumetric (V) TE coefficients for the solids discussed here. The systems are highlighted as follows: 0D (red and yellow), 1D (black), and 2D (grey). Errors in the TE coefficients are shown in Table S15.

Impact of dimensionality on TE

The effect of dimensionality on TE can be garnered by examining a series of 0D-2D solids while keeping the bipyridine constant. In comparing the 0D to 1D solids, expansion along X_1 in the 0D solid is larger than (or approximately equal to, in one case) the TE of the 1D solid. This is because

in the 1D solids, the strong hydrogen bonds run infinitely in 1D instead of as isolated 0D pairs (see Figure 1). The expansion along X_2 in the 0D solid is also larger than (or approximately equal to, in one case) the TE of the 1D solid. For both the 0D and 1D solids, the X_2 direction is sustained by weaker hydrogen bonds (C-H···O). However, in the 1D solids, the infinite chains of carboxylic acid donor molecules afford more C-H···O contact points within the X_2 direction when compared to the 0D solids. The isolated acid groups in the 0D solids have less contacts along X_2 , weakening the direction and causing larger TE (Figure S31). The 2D solids exhibit biaxial ZTE along X_1 and X_2 because both directions comprise the strong hydrogen bonds. Thus, as the supramolecular hydrogen-bonding dimensionality increases, the corresponding TE along those dimensions decreases, analogous to the behavior of covalently-bonded carbon allotropes.

The 2D solid-state supramolecular materials discussed here exhibit biaxial ZTE within the hydrogen-bonded sheet, which is coupled with colossal PTE along X₃. The 2D solids containing bpe and azo also exhibit solid-state motion with change in temperature, which also contributes to the colossal PTE along X₃. Due to the anharmonicity in the short and strong hydrogen bonds, the motion in the 2D solids results in the transverse vibrational mode dominating over the longitudinal mode, to afford the slight NTE within the 2D hydrogen-bonded sheet. ^{61, 62} The 2D hydrogen-bonded solids exhibit significant anisotropic TE along the π-stacked direction (Figure 8), and the coefficients of TE along this direction are 226 MK⁻¹ (bpeth), 218 MK⁻¹ (azo), and 164 MK⁻¹ (bpe). These coefficients are on par with or higher than many of the reported TE coefficients for multicomponent supramolecular solids assembled via noncovalent interactions (Table S22). The 2D materials graphite and black phosphorus also exhibit anisotropic TE along the interlayer direction; however, the coefficients in the 2D hydrogen-bonded materials described here are significantly higher than other 2D materials. The experimental anisotropic coefficients for graphite and black

phosphorous are ca. 27 and 40 MK^{-1} , ^{32, 41} while the 2D hydrogen-bonded materials here are ca. 200 MK^{-1} .

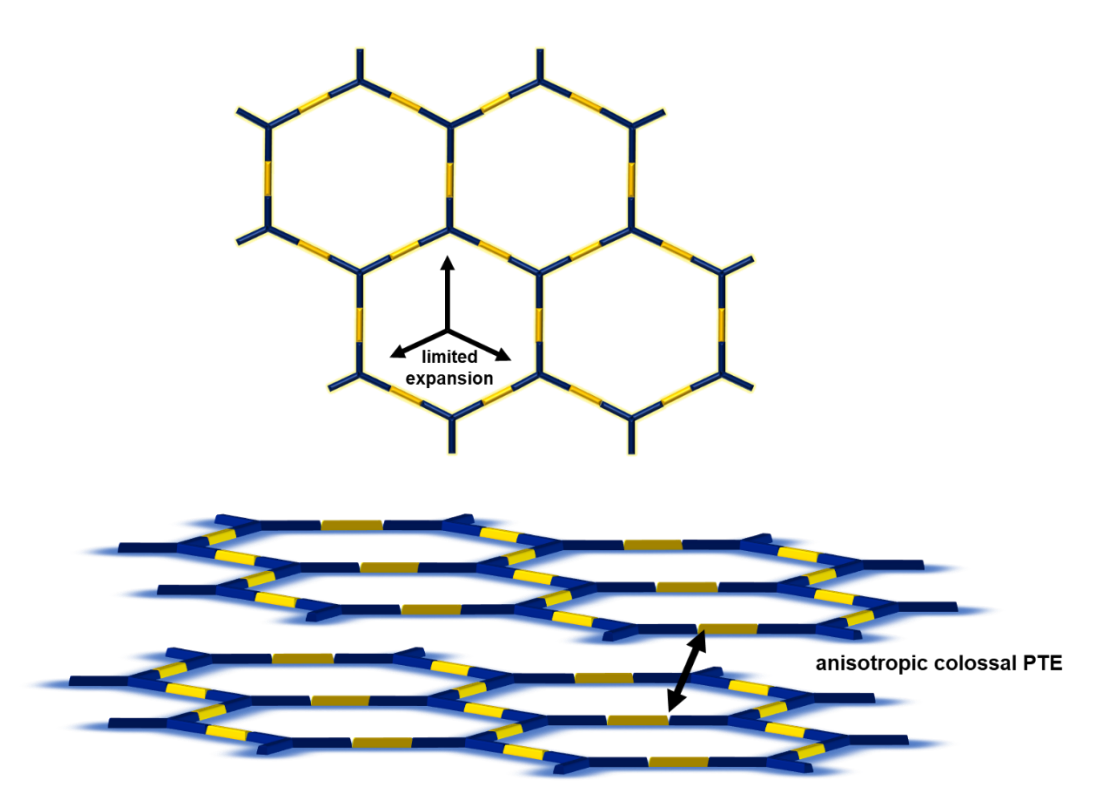


Figure 8. Representation of TE behavior in 2D supramolecular materials highlighting limited expansion within the 2D sheets and anisotropic, colossal PTE between the 2D sheets.

Since all the hydrogen-bonded solids here are sustained by π -stacking interactions along the third dimension, we did not necessarily expect to control the volumetric TE behavior. However, for solids containing bpe and bpeth, the volumetric TE does indeed decrease with increasing dimensionality (Figure 7). The trend breaks slightly for the 2D solid containing azo because of the significant TE and molecular motion along X_3 compared to the other azo solids in the series (Figure 7).

Conclusions

In this study, for the first time, we have shown that by systematically controlling the dimensionality of supramolecular solids, TE can be directly controlled in a manner analogous to carbon allotropes. Specifically, increasing the hydrogen-bonding dimensionality results in limited TE along the directions the hydrogen bonds lie. Thus, the 0D hydrogen-bonded solids, which are analogus to fullerene, undergo the most TE. The 2D hydrogen-bonded solids, which are analogus to graphite, exhibit the least TE. In the 2D solids described here, biaxial ZTE occurred within the hydrogen-bonded sheets and anisotropic, colossal PTE was achieved along the π -stacked direction. Notably, the contribution of dynamic motion in the materials is a unique feature and enhances the overall TE in the 2D azo based solid. Achieving anisotropic behavior in solid materials is desirable, yet challenging. The hierarchical materials design strategy described here offers a method for not only achieving anisotropic behaviors, but also controlling properties through systematic selfassembly. Given the broad applicability of 2D solids in advanced material applications (e.g., electronics) and the anisotropic behavior attained, this study opens the door for investigating supramolecular solid-state materials synthesized using other classes of noncovalent interactions for self-assembly.

ASSOCIATED CONTENT

Supporting Information. Experimental details, single-crystal X-ray diffraction data, thermal expansion data and analysis, ¹H NMR spectra, powder X-ray diffraction data. The following files are available free of charge.

Supporting information file (PDF)

Accession Codes. CCDC 2268605-2268646 contains crystallographic data for the 0D and 2D solids. CCDC 1955381-1955386 and CCDC 1955395-1955406 contains crystallographic data for the 1D solids.

AUTHOR INFORMATION

Corresponding Author

*Email: kristin.hutchins@ttu.edu

Author Contributions

The manuscript was written through contributions of all authors. All authors have given approval to the final version of the manuscript.

ACKNOWLEDGMENT

K.M.H. gratefully acknowledges financial support from the National Science Foundation DMR-2045506.

REFERENCES

- (1) Megaw, H. D. Crystal structures and thermal expansion. *Mater. Res* 1971, 6, 1007-1018.
- (2) Lee, A. v. d.; Dumitrescu, D. G. Thermal expansion properties of organic crystals: a CSD study. *Chem. Sci.* **2021**, *12*, 8537-8547.
- (3) Barrera, G. D.; Bruno, J. A. O.; Barron, T. H. K.; Allan, N. L. Negative thermal expansion. *J. Phys.: Condens. Matter* **2005**, *17*, R217-R252.
- (4) Das, D.; Jacobs, T.; Barbour, L. J. Exceptionally large positive and negative anisotropic thermal expansion of an organic crystalline material. *Nat. Mater.* **2010**, *9*, 36-39.
- (5) Chen, L.; Chen, X.; Ma, R.; Lin, K.; Li, Q.; Lang, J.-P.; Liu, C.; Kato, K.; Huang, L.; Xing, X. Thermal enhancement of luminescence for negative thermal expansion in molecular materials. *J. Am. Chem. Soc.* **2022**, *144*, 13688-13695.
- (6) Yu, C.; Lin, K.; Chen, X.; Jiang, S.; Cao, Y.; Li, W.; Chen, L.; An, K.; Chen, Y.; Yu, D.; Kato, K.; Zhang, Q.; Gu, L.; You, L.; Kuang, X.; Wu, H.; Li, Q.; Deng, J.; Xing, X. Superior zero thermal expansion dual-phase alloy via boron-migration mediated solid-state reaction. *Nat. Commun.* **2023**, *14*, 3135.
- (7) Li, S.; Takahashi, K.; Huang, R.-K.; Xue, C.; Kokado, K.; Hoshino, N.; Akutagawa, T.; Nishihara, S.; Nakamura, T. Multifunctional triggering by solid-phase molecular motion:

- Relaxor ferroelectricity, modulation of magnetic exchange interactions, and enhancement of negative thermal expansion. *Chem. Mater.* **2023**, *35*, 2421-2428.
- (8) Baxter, S. J.; Schneemann, A.; Ready, A. D.; Wijeratne, P.; Wilkinson, A. P.; Burtch, N. C. Tuning thermal expansion in metal—organic frameworks using a mixed linker solid solution approach. *J. Am. Chem. Soc.* **2019**, *141*, 12849-12854.
- (9) Wyk, L. M. v.; Loots, L.; Barbour, L. J. Tuning extreme anisotropic thermal expansion in 1D coordination polymers through metal selection and solid solutions. *Chem. Commun.* **2021**, *57*, 7693-7696.
- (10) Ramakrishnan, M.; Rajan, G.; Semenova, Y.; Lesiak, P.; Domanski, A.; Wolinski, T.; Boczkowska, A.; Farrell, G. The influence of thermal expansion of a composite material on embedded polarimetric sensors. *Smart Mater. Struct.* **2011**, *20*, 125002.
- (11) Khalil, A.; Karothu, D. P.; Naumov, P. Direct quantification of rapid and efficient single-stroke actuation by a martensitic transition in a thermosalient crystal. *J. Am. Chem. Soc.* **2019**, *141*, 3371-3375.
- (12) Niu, D.; Jiang, W.; Liu, H.; Zhao, T.; Lei, B.; Li, Y.; Yin, L.; Shi, Y.; Chen, B.; Lu, B. Reversible bending behaviors of photomechanical soft actuators based on graphene nanocomposites. *Sci. Rep.* **2016**, *6*, 27366.
- (13) Miller, W.; Smith, C. W.; Mackenzie, D. S.; Evans, K. E. Negative thermal expansion: a review. *J. Mater. Sci.* **2009**, *44*, 5441-5451.
- (14) Goodwin, A. L.; Kepert, C. J. Negative thermal expansion and low-frequency modes in cyanide-bridged framework materials. *Phy. Rev. B* **2005**, *71*, 140301.
- (15) Chen, J.; Hu, L.; Deng, J.; Xing, X. Negative thermal expansion in functional materials: controllable thermal expansion by chemical modifications. *Chem. Soc. Rev.* **2015**, *44*, 3522-3567.
- (16) Shi, J. D.; Pu, Z. J.; Wu, K. H.; Larkins, G. Composite materials with adjustable thermal expansion for electronic applications. *Mater. Res. Soc. Symp. Proc.* **1996**, *445*, 229-234.
- (17) Wang, C.; Dong, H.; Hu, W.; Liu, Y.; Zhu, D. Semiconducting π -conjugated systems in field-effect transistors: A material odyssey of organic electronics. *Chem. Rev.* **2012**, *112*, 2208-2267.
- (18) Juneja, N.; Shapiro, N. M.; Unruh, D. K.; Bosch, E.; Groeneman, R. H.; Hutchins, K. M. Controlling Thermal Expansion in Supramolecular Halogen-Bonded Mixed Cocrystals through Synthetic Feed and Dynamic Motion. *Angew. Chem. Int. Ed.* **2022**, e202202708.
- (19) Bushuyev, O. S.; Friščić, T.; Barrett, C. J. Controlling dichroism of molecular crystals by cocrystallization. *Cryst. Growth Des.* **2016**, *16*, 541–545.
- (20) Rather, S. A.; Saraswatula, V. G.; Sharada, D.; Saha, B. K. Influence of molecular width on the thermal expansion in solids. *New J. Chem.* **2019**, *43*, 17146-17150.
- (21) Khuong, T.-A. V.; Nunez, J. E.; Garcia-Garibay, M. A. Crystalline molecular machines: A quest toward solid-state dynamics and function. *Acc. Chem. Res.* **2006**, *39*, 413-422.
- (22) Feng, L.; Astumian, R. D.; Stoddart, J. F. Controlling dynamics in extended molecular frameworks. *Nat. Rev. Chem.* **2022**, *6*, 705-725.
- (23) Koupepidou, K.; Nikolayenko, V. I.; Sensharma, D.; Bezrukov, A. A.; Vandichel, M.; Nikkhah, S. J.; Castell, D. C.; Oyekan, K. A.; Kumar, N.; Subanbekova, A.; Vandenberghe, W. G. Tan, K.; Parkers, L. L. Zarrandte, M. L. Orandtenson and J. H. d.; Grandtenson and J. H. d.; Gr
- G.; Tan, K.; Barbour, L. J.; Zaworotko, M. J. One atom can make all the difference: Gas-induced phase transformations in bisimidazole-linked diamondoid coordination networks. *J. Am. Chem. Soc.* **2023**, *145*, 10197-10207.

- (24) Donoshita, M.; Yoshida, Y.; Hayashi, M.; Ikeda, P. R.; Tanaka, P. S.; Yamamura, Y.; Saito, P. K.; Kawaguchi, D. S.; Sugimoto, D. K.; Kitagawa, P. H. Various stacking patterns of two-dimensional molecular assemblies in hydrogen-bonded cocrystals: Insight into competitive intermolecular interactions and control of stacking patterns. *Angew. Chem. Int. Ed.* **2021**, *60*, 22839-22848.
- (25) Palmer, L. C.; Stupp, S. I. Molecular self-assembly into one-dimensional nanostructures. *Acc. Chem. Res.* **2008**, *41*, 1674-1684.
- (26) Kulkarni, C.; Berrocal, J. A.; Lutz, M.; Palmans, A. R. A.; Meijer, E. W. Directing the solid-state organization of racemates via structural mutation and solution-state assembly processes. *J. Am. Chem. Soc.* **2019**, *141*, 6302-6309.
- (27) Dreher, M.; Dombrowski, P. M.; Tripp, M. W.; Münster, N.; Koert, U.; Witte, G. Shape control in 2D molecular nanosheets by tuning anisotropic intermolecular interactions and assembly kinetics. *Nat. Commun.* **2023**, *14*, 1554.
- (28) Yusov, A.; Dillon, A. M.; Ward, M. D. Hydrogen bonded frameworks: smart materials used smartly. *Mol. Syst. Des. Eng.* **2021**, *6*, 756-778.
- (29) Scott, H. S.; Ogiwara, N.; Chen, K.-J.; Madden, D. G.; Pham, T.; Forrest, K.; Space, B.; Horike, S.; Perry Iv, J. J.; Kitagawa, S.; Zaworotko, M. J. Crystal engineering of a family of hybrid ultramicroporous materials based upon interpenetration and dichromate linkers. *Chem. Sci.* **2016**, *7*, 5470-5476.
- (30) Kitaigorodsky, A. I. Molecular crystals and molecules; New York: Academic Press, 1973.
- (31) Wang, S.; Tambraparni, M.; Qiu, J.; Tipton, J.; Dean, D. Thermal expansion of graphene composites. *Macromolecules* **2009**, *42*, 5251-5255.
- (32) Zhao, L.; Tang, J.; Zhou, M.; Shen, K. A review of the coefficient of thermal expansion and thermal conductivity of graphite. *New Carbon Mater.* **2022**, *37*, 544-555.
- (33) Nelson, J. B.; Riley, D. P. The thermal expansion of graphite from 15°C. to 800°C.: part I. Experimental. *Proc. Phys. Soc.* **1945**, *57*, 477-486.
- (34) Jacobson, P.; Stoupin, S. Thermal expansion coefficient of diamond in a wide temperature range. *Diam. Relat. Mater.* **2019**, *97*, 107469.
- (35) Mathews, C. K.; Rajagopalan, S.; Kutty, K. V. G.; Asuvathraman, R.; Sivaraman, N.; Srinivasan, T. G.; Rao, P. R. V. Crystal structures and thermal expansion of fullerenes. *Solid State Commun.* **1993**, *85*, 377-379.
- (36) Ye, X.; Qi, M.; Chen, M.; Zhang, L.; Zhang, J. Zero to three dimension structure evolution from carbon allotropes to phosphorus allotropes. *Adv. Mater. Interfaces* **2023**, *10*, 2201941.
- (37) Sun, H.; Liu, G.; Li, Q.; Wan, X. G. First-principles study of thermal expansion and thermomechanics of single-layer black and blue phosphorus. *Phys. Lett. A* **2016**, *380*, 2098-2104.
- (38) Aierken, Y.; Çakır, D.; Sevik, C.; Peeters, F. M. Thermal properties of black and blue phosphorenes from a first-principles quasiharmonic approach. *Phys. Rev. B* **2015**, *92*, 081408.
- (39) Sansone, G.; Karttunen, A. J.; Usvyat, D.; Schütz, M.; Brandenburg, J. G.; Maschio, L. On the exfoliation and anisotropic thermal expansion of black phosphorus. *Chem. Commun.* **2018**, *54*, 9793-9796.
- (40) Rodrigues, J. E. F. S.; Gainza, J.; Serrano-Sánchez, F.; López, C.; Dura, O. J.; Nemes, N.; Martinez, J. L.; Huttel, Y.; Fauth, F.; Fernández-Diaz, M. T.; Biškup, N.; Alonso, J. A. Structural features, anisotropic thermal expansion, and thermoelectric performance in bulk black phosphorus synthesized under high pressure. *Inorg. Chem.* **2020**, *59*, 14932-14943.

- (41) Henry, L.; Svitlyk, V.; Mezouar, M.; Sifré, D.; Garbarino, G.; Ceppatelli, M.; Serrano-Ruiz, M.; Peruzzini, M.; Datchi, F. Anisotropic thermal expansion of black phosphorus from nanoscale dynamics of phosphorene layers. *Nanoscale* **2020**, *12*, 4491-4497.
- (42) Geim, A. K.; Novoselov, K. S. The rise of graphene. *Nature. Mater.* **2007**, *6*, 183-191.
- (43) Li, W.; Qian, X.; Li, J. Phase transitions in 2D materials. Nat. Rev. Mater. 2021, 6, 829-846.
- (44) Yang, F.; Cheng, S.; Zhang, X.; Ren, X.; Li, R.; Dong, H.; Hu, W. 2D organic materials for optoelectronic applications. *Adv. Mater.* **2018**, *30*, 1702415.
- (45) Yan, X.; Zhao, Y.; Cao, G.; Li, X.; Gao, C.; Liu, L.; Ahmed, S.; Altaf, F.; Tan, H.; Ma, X.; Xie, Z.; Zhang, H. 2D organic materials: Status and challenges. *Adv. Sci.* **2023**, *10*, 2203889.
- (46) Das, R. K.; Aggarwal, H.; Barbour, L. J. Anomalous anisotropic thermal expansion in a one-dimensional coordination polymer driven by conformational flexibility. *Inorg. Chem.* **2015**, *54*, 8171-8173.
- (47) Hutchins, K. M.; Groeneman, R. H.; Reinheimer, E. W.; Swenson, D. C.; MacGillivray, L. R. Achieving dynamic behaviour and thermal expansion in the organic solid state via cocrystallization. *Chem. Sci.* **2015**, *6*, 4717-4722.
- (48) Saraswatula, V. G.; Bhattacharya, S.; Saha, B. K. Can the thermal expansion be controlled by varying hydrogen bond dimensionality in polymorphs? *New J. Chem.* **2015**, *39*, 3345-3348.
- (49) Bhattacharya, S. Thermal expansion and dimensionality of a hydrogen bond network: a case study on dimorphic oxalic acid. *CrystEngComm* **2020**, *22*, 7896-7902.
- (50) Bhattacharya, S.; Saha, B. K. Interaction Dependence and Similarity in Thermal Expansion of a Dimorphic 1D Hydrogen-Bonded Organic Complex. *Cryst. Growth Des.* **2013**, *13*, 3299-3302.
- (51) Saha, B. K. Thermal expansion in organic crystals. J. Indian Inst. Sci. 2017, 97, 177–191.
- (52) Thewlis, J.; Davey, A. R. XL. Thermal expansion of diamond. *Philos. Mag.* **1956**, *1*, 409-414.
- (53) Harada, J.; Ogawa, K. Pedal motion in crystals. *Chem. Soc. Rev.* **2009**, *38*, 2244-2252.
- (54) Hutchins, K. M.; Unruh, D. K.; Verdu, F. A.; Groeneman, R. H. Molecular pedal motion influences thermal expansion properties within isostructural hydrogen-bonded co-crystals. *Cryst. Growth Des.* **2018**, *18*, 566-570.
- (55) Ding, X.; Unruh, D. K.; Groeneman, R. H.; Hutchins, K. M. Controlling thermal expansion within mixed cocrystals by tuning molecular motion capability. *Chem. Sci.* **2020**, *11*, 7701-7707.
- (56) Cliffe, M. J.; Goodwin, A. L. PASCal: a principal axis strain calculator for thermal expansion and compressibility determination. *J. Appl. Cryst.* **2012**, *45*, 1321-1329
- (57) Weyna, D. R.; Shattock, T.; Vishweshwar, P.; Zaworotko, M. J. Synthesis and structural characterization of cocrystals and pharmaceutical cocrystals: Mechanochemistry vs slow evaporation from solution. *Cryst. Growth Des.* **2008**, *9*, 1106-1123.
- (58) Ding, X.; Juneja, N.; Crawford, A. W.; Reinheimer, E. W.; Unruh, D. K.; Hutchins, K. M. Influence of multiple hydrogen bonds on thermal expansion within and between two-dimensional hydrogen-bonded sheets. *Cryst. Growth Des.* **2019**, *19*, 7380-7384.
- (59) Shattock, T. R.; Vishweshwar, P.; Wang, Z.; Zaworotko, M. J. 18-Fold interpenetration and concomitant polymorphism in the 2:3 co-crystal of trimesic acid and 1,2-bis(4-pyridyl)ethane. *Cryst. Growth Des.* **2005**, *5*, 2046-2049.
- (60) Goodwin, A. L.; Calleja, M.; Conterio, M. J.; Dove, M. T.; Evans, J. S. O.; Keen, D. A.; Peters, L.; Tucker, M. G. Colossal positive and negative thermal expansion in the framework material Ag 3[Co(CN)₆]. *Science* **2008**, *319*, 794-797.

- (61) Chapman, K. W.; Chupas, P. J.; Kepert, C. J. Direct observation of a transverse vibrational mechanism for negative thermal expansion in Zn(CN)₂: An atomic pair distribution function analysis. *J. Am. Chem. Soc.* **2005**, *127*, 15630-15636.
- (62) Michel, K. H.; Costamagna, S.; Peeters, F. M. Theory of anharmonic phonons in two-dimensional crystals. *Phy. Rev. B* **2015**, *91*, 134302.

Table of Contents

